Time-resolved spectroscopic studies of the ultrafast photoisomerisation reaction in cyanobacteriochrome Tlr0924

Contact *Derren.heyes@manchester.ac.uk*

Samantha J. O. Hardman
Manchester Institute of Biotechnology, University of Manchester, 131 Princess Street, Manchester M1 7DN, UK

Anna F. E. Hauck
Manchester Institute of Biotechnology, University of Manchester, 131 Princess Street, Manchester M1 7DN, UK

Derren J. Heyes
Manchester Institute of Biotechnology, University of Manchester, 131 Princess Street, Manchester M1 7DN, UK

Nigel S. Scrutton
Manchester Institute of Biotechnology, University of Manchester, 131 Princess Street, Manchester M1 7DN, UK

Greg M. Greetham
Central Laser Facility, STFC Rutherford Appleton Laboratory, Harwell Campus, Didcot, UK

Ian P. Clark
Central Laser Facility, STFC Rutherford Appleton Laboratory, Harwell Campus, Didcot, UK

Introduction

The coupling of photochemistry to protein chemical and structural change is crucial to biological light-activated signalling mechanisms. This is typified by the cyanobacteriochromes (CBCRs), which are members of the phytochrome superfamily of photoreceptors [1]. The CBCRs exhibit a high degree of spectral diversity, collectively spanning the entire visible spectrum. They mediate a variety of signalling responses in cyanobacteria by using a reversible photo-induced *E/Z* isomerisation of a sensory bilin chromophore [1]. The general protein structure is divided into domains, always including the photosensory chromophore binding GAF (cGMP-specific phosphodiesterase / adenylyl cyclase / FhlA protein) domain and one or more output domains (*e.g.* histidine kinase or GGDEF domain) [1, 2]. However, in contrast to the closely related phytochrome proteins, the individual GAF domains of CBCRs are able to autonomously undergo efficient, reversible, photoconversions [1-4]. Modulation of the bilin conjugated system is achieved by different tuning mechanisms, such as structural variations in the chromophore and/or breakup of the delocalized π-electron system. However, the photochemical mechanisms that allow this photosensory flexibility are only beginning to be understood and a kinetic description of the complete photocycle of a CBCR is still lacking.

Tlr0924 from *Thermosynechococcus elongatus* is a blue/green photoreceptor that belongs to the DXCF subgroup (containing the Asp-Xaa-Cys-Phe motif) of CBCRs [3]. In a process that has been observed previously in similar CBCRs [5, 6] the intrinsic GAF isomerase activity in Tlr0924 converts the phycocyanobilin (PCB) precursor chromophore to phycoviolobilin (PVB) incompletely on a timescale of days, resulting in a heterogeneous population with a final ratio of around 1:4 (Fig. 1A). The absorption spectrum is consequently composed of features originating from both the PVB and PCB chromophores (Fig. 1B). The Tlr0924 photocycle has been studied by visible absorption spectroscopy and circular dichroism and was shown to interconvert between blue-absorbing (Pb) and green-absorbing (Pg) states upon absorption of the relevant wavelength of light [3, 7]. The large spectral shift cannot be achieved by isomerisation alone, but is brought about by a second thioether linkage formed between the bilin C10 and Cys-499 in the protein DXCF motif [3, 7, 8]. The absorption maxima of the Pb ground states are spectrally identical for PCB and PVB in the visible region because the second thioether linkage restricts the photochemically relevant, conjugated system to the C and D rings. Blue light absorption will therefore inevitably activate both photoconversions, resulting in green-absorbing PVB photoproduct and red-absorbing (Pr) PCB photoproduct, with their conjugated systems extended to ring B and rings A and B, respectively. The photoproducts still exhibit a significant spectral overlap and green light absorption returns both chromophores to their blue-absorbing states. However, far-red illumination will convert only PCB back to the Pb state. The individual spectral contributions can be isolated by this sequential photoconversion permitting further studies [3, 8] or the states without the second thioether linkage to the protein can be visualised by (permanent) acid denaturation [3, 9, 10].

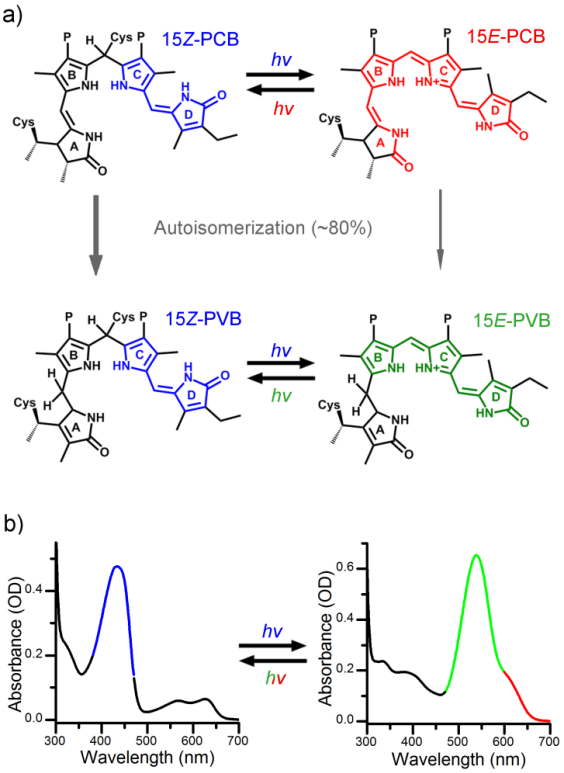

Figure 1. A. Structures, and B. related absorption spectra of the $^{15Z\text{-}PVB}$Pb, $^{15E\text{-}PVB}$Pg, $^{15Z\text{-}PCB}$Pb, and $^{15E\text{-}PCB}$Pr chromophores of Tlr0924. The PCB and PVB populations autoisomerise to yield a mixture of the two chromophores, which can be converted between photostates with the relevant wavelength of light

The ultrafast photoisomerization reaction dynamics of the GAF domain of Tlr0924 have previously been investigated by exciting the two parallel photoconversions simultaneously, which has allowed the primary photoproducts to be identified [11]. In the present work we have used a combination of time-resolved UV-vis and IR spectroscopy to characterise the *Z* to *E* and *E* to *Z* photoisomerisation reactions of the full-length protein. The experimental isolation of the PVB and PCB populations allowed a detailed assignment of the ultrafast reaction dynamics for both processes.

MATERIALS AND METHODS

Protein expression and purification. The gene for full-length Tlr0924 was synthesised (Genscript Inc.) and cloned into the pBAD-HisB expression plasmid. Full-length Tlr0924 was expressed as a recombinant holoprotein by using a dual plasmid *E. coli* expression system [12, 13]. BL21(DE3) containing a PCB biosynthetic expression plasmid (pCOLADuet-1 (Novagen) HO1 PcyA) for chromophore production was cotransformed with the pBAD-HisB-Tlr0924 plasmid. The protein was purified by a 2-step method employing Nickel affinity chromatography followed by gel filtration in a phosphate based buffer system [100 mM sodium-potassium phosphate, 300 mM NaCl, pH 7] supplemented with 200 mM L-histidine for elution. Pure sample was flash-frozen and stored at -80 °C. The chromophore content was approximately 80% PVB and 20% PCB, as indicated by UV/Vis spectroscopy, and based on published conversion rates this ratio can be assumed to remain constant over the course of the experiments [3].

Time-resolved UV-vis measurements. The laser system used in the visible transient absorption measurements consists of a Ti:sapphire amplifier (hybrid Coherent Legend Elite-F-HE) pumped by a Q-switched Nd:YLF laser (Positive light Evolution-30) and seeded by a Ti:sapphire laser (Spectra Physics Mai Tai). The amplifier output (1 kHz repetition rate, 800 nm centre wavelength, ~120 fs pulse duration) was split to generate the pump and probe beams. A non-collinear optical parametric amplifier (Light Conversion TOPAS White) was used to generate the pump beam centered at 435 nm or 530 nm, with a full width at half maximum intensity of ca. 10 nm. Excitation energies of 0.75-1 μJ were used with a beam diameter of around 150 μm, which yielded pump fluences of 4.2-5.7 mJ/cm^2. The accessible region of the spectrum was maximised by adjusting the polarisations of pump and probe to be perpendicular, and using a polariser before the detectors to eliminate a large proportion of the scattered pump light. Data collected with a depolarised pump beam yielded kinetics and spectra similar, although the intensity of the negative stimulated emission peak varied between the samples, thus we assume any polarisation effects will not affect the model derived from these data. The probe beam consisted of a white light continuum generated in a rastered CaF_2 crystal. The broad band pump-probe transient absorbance spectrometer 'Helios' (Ultrafast Systems LLC) had a time resolution of approximately 0.2 ps. Absorbance changes were monitored between 350 and 700 nm with data points collected randomly over the 3 ns time frame. Samples were contained in stirred 2 mm path length quartz cuvettes (optical density (OD) at 535 nm = 0.5). During the measurements the samples were continuously illuminated using a cold light source (Schott KL1500) and the appropriate bandpass filter (Andover Corp). For the measurements where samples were excited at 435 nm illumination at 540 nm was used to regenerate the PVB and PCB Pb states from their corresponding Pg and Pr states, and 640 nm illumination used to regenerate the PCB Pb state from the Pr state. For the measurements where samples were excited at 530 nm illumination at 435 nm was used to regenerate the PVB and PCB Pr and Pg states from their corresponding Pb states, and simultaneous 640 nm illumination used to regenerate the PCB Pb state from the Pr state, this left only the PVB Pg state to be excited by the pump laser.

Time-resolved IR measurements. Time-resolved IR spectroscopy was carried out at the Ultra facility (CLF, STFC Rutherford Appleton Laboratory, UK), which uses a 10 kHz repetition rate laser and has a time resolution of around 100 fs (22). Samples were flowed through a 100 μm CaF_2 measurement cell and the sample holder rastered to avoid sample damage. In addition, the samples were regenerated by continuous sample illumination with a cold light source as described above. An excitation energy of 0.6 uJ at either 435 nm or 530 nm was used, the beam diameter was around 150 μm, yielding a pump fluence of 4.3 mJ/cm^2, and the excitation beam was set at the magic angle with respect to the IR probe beam. Data were collected for approximately half an hour per dataset, the spectral resolution was ~3 cm^{-1}, pixel to wavenumber calibration was performed as described previously [14].

Global analysis. The transient absorption and laser flash photolysis 3D datasets were analyzed globally using the open-source software Glotaran [15]. This procedure reduces the matrix of time, wavelength, and change in absorbance to one or more exponentially decaying time components, each with a corresponding difference spectrum. The visible and IR ultrafast transient absorption data were fitted from 0.3 and 0.2 ps, respectively, to avoid any contributions from coherent artifacts [16].

RESULTS AND DISCUSSION

Ultrafast transient UV-Visible dynamics of the Z to E photoisomerisation. Previous measurements have shown that the photoisomerisation of the bilin cofactor occurs on an ultrafast timescale for both phytochromes and the isolated GAF domain of CBCRs (15,16,19,26-32). Here, ultrafast transient absorption spectroscopy has been used to study both the *Z* to *E* and *E* to *Z* photoisomerisation processes in the full-length Tlr0924 CBCR. Laser pulses at 435 nm were used to induce photoconversion of the $^{15Z\text{-}PVB}$Pb and $^{15Z\text{-}PCB}$Pb populations to the $^{15E\text{-}PVB}$Pg and $^{15E\text{-}PCB}$Pr populations, respectively. Continuous illumination with green light (540 nm) during data collection returned both of the 'final' $^{15E\text{-}PVB}$Pg and $^{15E\text{-}PCB}$Pr populations to their corresponding Pb states. Therefore excitation at 435 nm initiated the photoisomerisation of a mixture of both PCB and PVB Pb states. However, as Tlr0924 exists as a heterogeneous population of PVB and PCB in a ratio of approximately 4:1 the majority of the time-dependent absorption changes are dominated by PVB (approximately 80 % of the signal). Further separation of the species was made possible by illumination with red light (640 nm) during data collection, which converted only the $^{15E\text{-}PCB}$Pr population to the Pb state, leaving the PVB population in the Pg state. In this case, the majority of signal after excitation at 435 nm originated from PCB only.

Using the conditions defined above, ultrafast transient absorption difference spectra were measured for both the predominantly PVB (hereafter termed 'PVB') and the predominantly PCB (hereafter termed 'PCB') forward reactions (Figs. 2a and 3a). In both cases, there is a bleach of the main ground state absorption band (GSB) at ~436 nm, which is flanked by broad overlapping positive excited state absorption (ESA) signals. We also observed a small ~510 nm stimulated emission (SE) band at very early times, and a small negative feature at ~640 nm, which likely corresponds to the bleach of a previously observed ground state absorption peak attributed to a small amount of inactive or modified protein [7]. On the sub-ps to 3 ns timescale monitored in these experiments the magnitude of the GSB is reduced and appears to slightly red-shift. The features in the red region of the spectrum disappear simultaneously and result in a broad positive feature spanning the entire 500 - 800 nm region at 3 ns. The data collected for the 'PCB' sample show very similar spectral features to the 'PVB'

sample although the SE band at ~510 nm is more pronounced for the 'PCB' sample, and appears to be slightly red shifted. This may be due to contamination of the signal by a small amount of PVB Pg to Pb photoconversion, which would result in a bleach feature at 532 nm. The bilin structures of the two chromophores are broadly similar, with the conjugated systems being identical in PCB and PVB, hence photoexcitation is likely to result in correspondingly similar excited states and primary photoproducts.

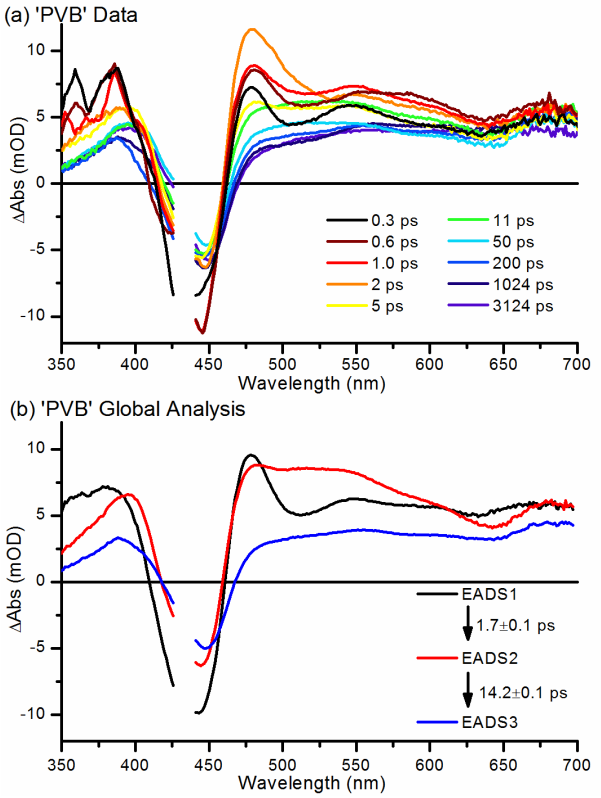

Figure 2. (a) Ultrafast transient absorption spectra, collected after excitation at 435 nm, at selected time points for 'PVB' samples, where Pb states were constantly regenerated with green light. (b) Global analysis of the ultrafast transient absorption data for the 'PVB' samples yielded 3 evolution associated difference spectra (EADS) which sequentially interconvert.

The datasets were analysed globally using a sequential model to give rise to evolution associated difference spectra (EADS), which represent the spectral evolution as a function of sequential exponential time constants rather than actual spectra of populations (Figs. 2b and 3b). In both the 'PVB' and 'PCB' datasets a good fit was achieved with 3 components and the resulting EADS were very similar for both samples. There are slight differences in the resulting lifetimes. This is almost certainly due to the small amount of signal contamination from the PVB Pg to Pb photoconversion in the 'PCB' dataset. The initial spectra, EADS1, show strong GSB and SE features, and a broad ESA, which rapidly decay in ~2 ps to the second spectra, EADS2. These spectra still contain a strong GSB feature and broad ESA, but no obvious SE. In the final component, EADS3, which grows in from EADS2 with a lifetime of ~10 ps, the GSB is still present, although red-shifted by ~5 nm compared to the previous components. This apparent shift is likely to be due to the appearance of a new positive feature at ~415 nm, corresponding to an isomerised, but still Cys-bound, intermediate [3, 7].

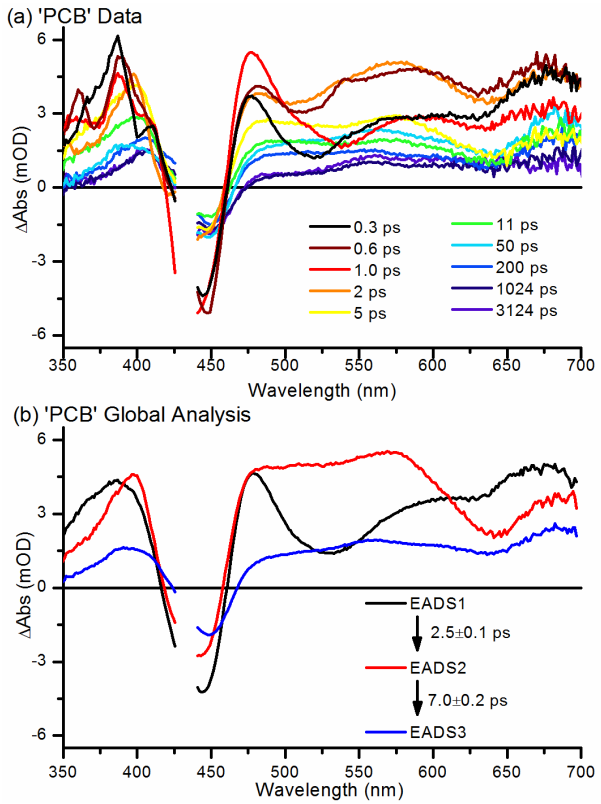

Figure 3. (a) Ultrafast transient absorption spectra, collected after excitation at 435 nm, at selected time points for 'PCB' samples where the Pb states were constantly regenerated with red light. (b) Global analysis of the ultrafast transient absorption data for the 'PCB' samples yielded 3 EADS which sequentially interconvert.

Ultrafast transient IR dynamics of the Z to E photoisomerisation. Ultrafast time resolved IR spectroscopy was used to probe structural changes in the mid-infrared region of the electromagnetic spectrum after initiation of the photoisomerisation reaction by 435 nm laser pulses. The difference spectra were qualitatively similar for both samples although the amplitude was reduced by approximately a third for the 'PCB' sample, reflecting the lower relative concentration of PCB compared to PVB (Figs. 4a and 5a). Consistent with visible ultrafast transient absorbance measurements, global analysis revealed that the data could be decomposed into 3 exponentially decaying species with lifetimes of τ = 3, 22, and 'infinite' ps and τ = 2, 17, and 'infinite' ps, for the 'PVB' and 'PCB' samples respectively (Figs 4b and 5b).

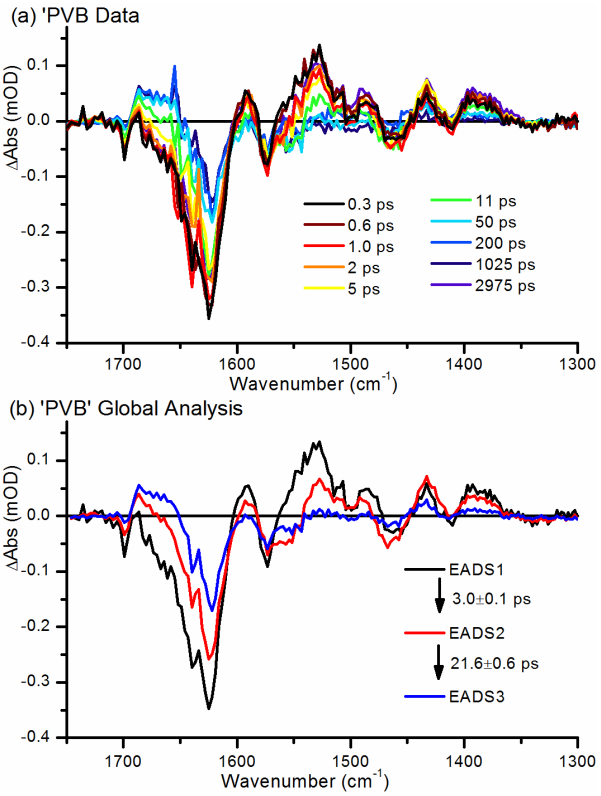

Figure 4. (a) Ultrafast transient IR absorption spectra, collected after excitation at 435 nm, at selected time points for 'PVB' samples, where Pb states were constantly regenerated with green light. (b) Global analysis of the ultrafast transient absorption data for the 'PVB' samples yielded 3 EADS which sequentially interconvert.

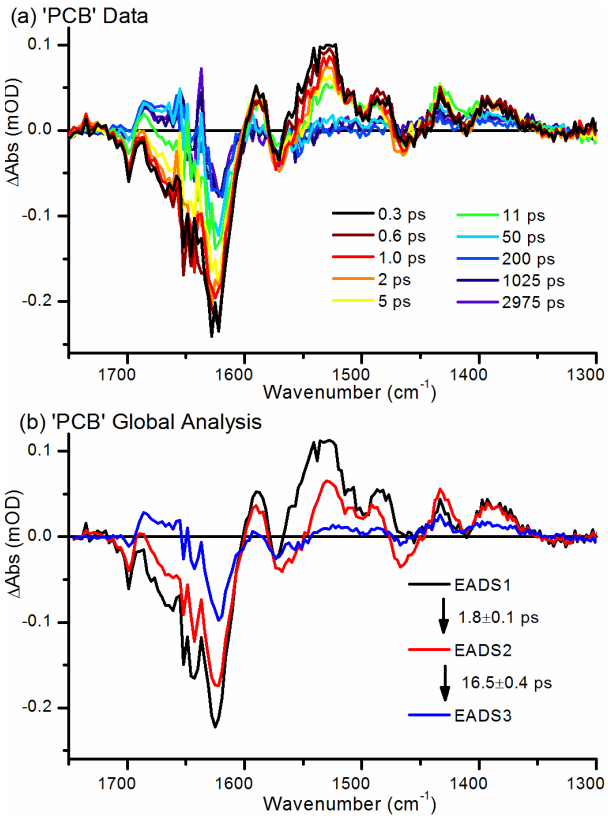

Figure 5. (a) Ultrafast transient IR absorption spectra, collected after excitation at 435 nm, at selected time points for 'PCB' samples where the Pb states were constantly regenerated with red light. (b) Global analysis of the ultrafast transient absorption data for the 'PCB' samples yielded 3 EADS which sequentially interconvert.

A number of previous studies on the related phytochrome proteins allow confident assignments to be made of the features in the difference spectra shown in Figs. 4 and 5. The largest ground state bleach (negative) features occur at ~1624 and ~1640 cm^{-1}, which correspond to C=C stretches in the C and D, and A and B rings, respectively [17, 18]. The small negative feature at ~1700 cm^{-1} is likely to correspond to the bleach of the C=O stretching mode from ring D [19, 20]. The other significant bleaches at ~1573 cm^{-1} and ~1467 cm^{-1} are likely due to C=O and C=N stretches, respectively, both coupled to a N-H rocking motion [21]. The main differences between EADS1 and EADS2 are a general loss of intensity across the whole spectral window. Features that can be attributed to the isomerised intermediate can be observed in EADS3 and include the downshift of the D-ring C=O stretch from ~1700 to ~1686 cm^{-1}, implying a more strongly hydrogen bonded environment in the $^{15E\text{-}PVB}$Pb, compared to the $^{15Z\text{-}PVB}$Pb state. Previous ultrafast IR studies have reported similar downshifts of this bond frequency upon isomerization in Cph1 [22] and two bacteriophytochromes [19], but static measurements of phytochromes have reported the opposite effect [23, 24], demonstrating the complexity of this family of photoreceptors. The C=N stretch at ~1467 cm^{-1} may also be downshifted by the isomerisation to form the small positive feature at ~1433 cm^{-1} [21]. The changes to the C=C stretches in the 1600-1650 cm^{-1} region are difficult to deconvolute, but it seems likely that the 1640 cm^{-1} feature originating from rings A and B will not change, whereas the ~1624 cm^{-1} feature from rings C and D may shift upon photoisomerisation.

The combination of ultrafast visible and IR transient absorption data leads us to suggest the scheme as shown in Fig. 6 for the photoisomerisation of the 15*Z* species. Immediately following photoexcitation to the Franck-Condon region very fast relaxation occurs within the time resolution of our detection method (~0.2 ps). From the Franck-Condon region an energetically excited region of the S1 potential energy surface is populated, from which SE can occur to the ground state. In ~2 ps this state has relaxed to the energy minima of the S1 surface, and on a timescale of ~10 ps the system relaxes to either the 15*Z* or 15*E* isomers. After this photoisomerisation step the ^{15E}Pb intermediate can then progress to the final $^{15E\text{-}PVB}$Pg and $^{15E\text{-}PCB}$Pr states. This scheme is less complex than, but similar to, those proposed in a previous study on the GAF domain of Tlr0924 [11] and for the corresponding isomerisation process in the related Cph1 phytochrome, both of which are suggested to involve multiple intermediates on both excited state and ground state energy surfaces [18, 25, 26]. Previous studies on CBCRs involved only the GAF domain and it is possible that the full-length protein restricts the number of accessible states, resulting in the suggested simple mechanism. This would be a contrast to phytochrome systems, where even the full length protein demonstrates multiple intermediates in the reaction pathway [27-29]. The difference between the systems lies in the thioether linkage to the protein, which is lacking in phytochromes and may provide added stabilisation to the CBCR reaction intermediates.

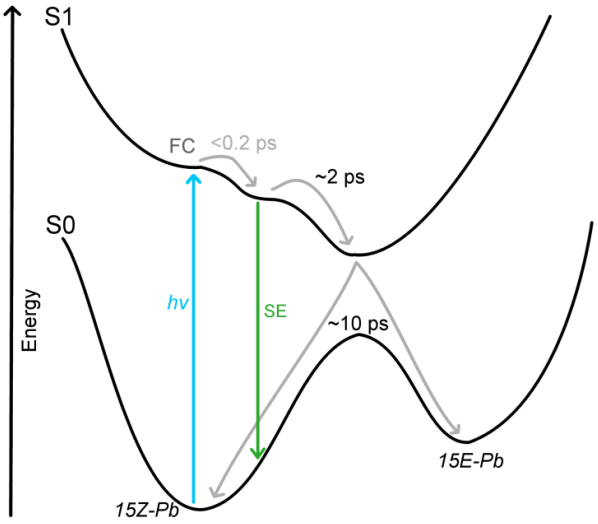

Figure 6. Scheme showing suggested ground and excited state energy surfaces and the processes which occur after photoexcitation at 435 nm. FC, Franck-Condon region, SE, stimulated emission

Ultrafast transient UV-Visible and IR dynamics of the Z to E photoisomerisation. In order to isolate the initial photoreaction of only the PVB chromophore in Tlr0924 samples were constantly illuminated simultaneously with blue and red light and excited with a ~530 nm pulsed laser as described in the methods section. The comparatively small population of the PCB chromophore combined with the selective wavelength constant illumination allows almost complete isolation of the PVB photodynamics.

The ultrafast transient absorption data collected for the initial steps of the PVB photoconversion are shown in Fig. 7a. Within the time resolution of the experiment (0.2 ps) two major spectral features appear: a large negative feature at ~530 nm, which can be assigned to the GSB of the Pg state, and a positive features at ~670 nm, which can be assigned to ESA of the Pg state. Within 5 ps these signals have decayed almost completely, although the features described above are still distinguishable and a positive feature at ~550 nm appears. Global analysis was carried out in order to more accurately define the spectral intermediates and the timescales of interconversion between intermediate states. A model with 4 sequentially converting spectral components, the EADS, (Fig. 7b) was found to be a good fit to the data and broadly agreed with literature values for GAF domain only Tlr0924 [11]. There was also an obvious contribution from a negative feature at ~645 nm, which has previously been ascribed to inactive or modified protein [7].

The ultrafast IR TA data were collected over the same time range, using the same time steps as were used for the visible TA experiments. The data, shown in Fig. 8a display a relatively simple picture. There are 3 major negative features at 1402, 1606, and 1685 cm^{-1}, but no immediately apparent positive features. The closely-related phytochromes have been extensively studied in the mid-IR region, allowing assignment of these bleaches as N-H in plane bending modes of rings A and D [17, 30], C=C stretches in rings A and B [18, 30], and C=O stretches in ring D [19, 22], respectively. Global analysis of the dataset using a basic, sequential model yields time constants comparable to those found from the visible TA data (Fig. 8b). There are one fewer components required to fit the data, the resulting time constants are 3.6, 196, and 'infinite' ps.

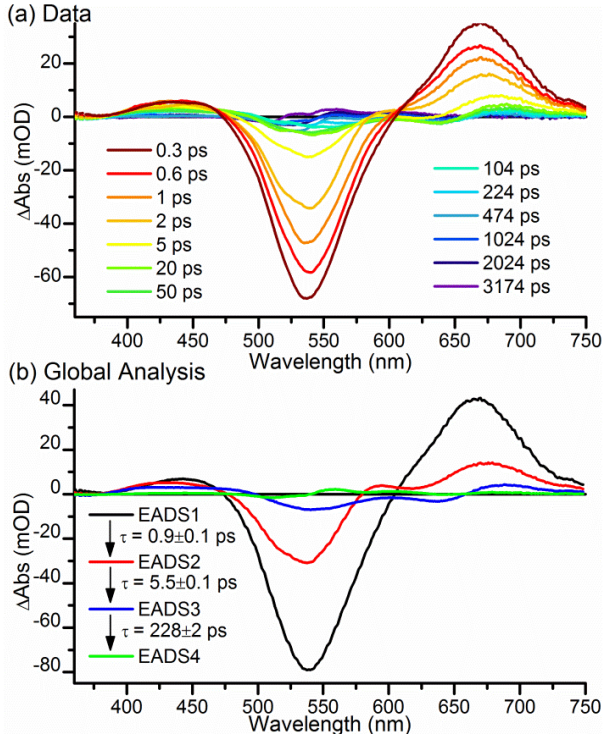

Figure 7. (a) Ultrafast visible transient absorption spectra at selected time points after excitation at 530 nm. The sample was constantly illuminated during data collection with blue and red light so the signals primarily originate from the Pg to Pb photoconversion of the PVB chromophore. (b) Global analysis of the ultrafast transient absorption data yielded 4 EADS which sequentially interconvert.

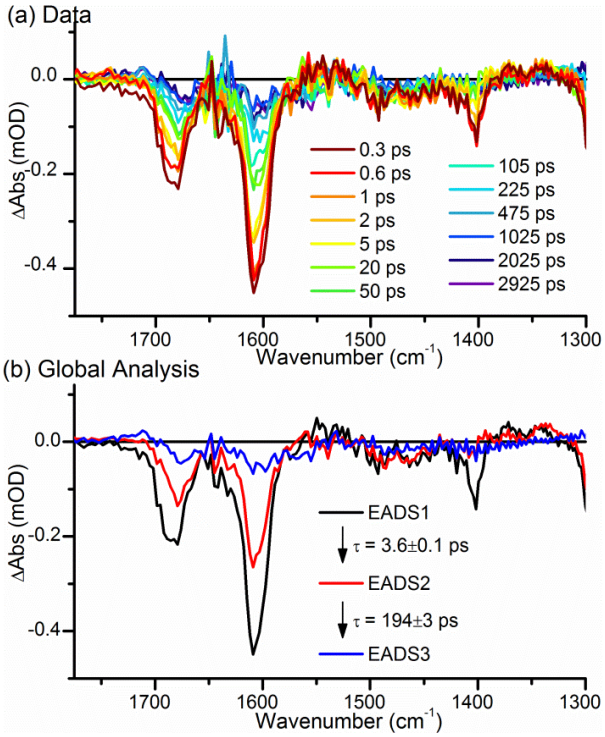

Figure 8. (a) Ultrafast IR transient absorption spectra at selected time points after excitation at 530 nm. The sample was constantly illuminated during data collection with blue and red light so the signals primarily originate from the Pb to Pb photoconversion of the PVB chromophore. (b) Global analysis of the ultrafast transient absorption data yielded 3 EADS which sequentially interconvert.

In order to more accurately model the ultrafast processes that occur upon photoisomerisation a more complex global analysis was performed (Fig. 9) to produce species associated difference spectra (SADS). In this model SADS1 evolves into non-decaying component SADS2. Independently, and in parallel to this process SADS3, representing the inactive protein, decays back to the ground state. In the case of the visible TA data an additional lifetime representing SADS1 decaying to the ground state was also fitted. The lifetimes produced by this model correlate extremely well between the visible and IR TA datasets. The SADS1 to SADS2 conversion lifetime was 3.6±0.1 ps in both datasets. The lifetime of SADS3 was fitted as 185±2 ps and 194±2 ps for the visible and IR TA data respectively. In the analysis of the visible TA SADS1 was found to relax to the ground state with a lifetime of 0.6±0.1 ps. This component was not resolved in the IR TA data, likely due to the similarity of the excited state and ground state vibrational spectra, with the poor signal-to-noise ratio of these data playing a role. The poor signal-to-noise ratio was due to both the low volume sample and the air bubbles in the sample, unavoidable due to the high flow rate necessary to avoid sample damage during the measurements.

In the case of the visible TA data it was assumed that any species in the photoconversion process would have Gaussian profiles, so a combination of Gaussian peaks were fitted to the resulting SADS (Fig. 4a-c). SADS1 is very similar in shape to the difference spectra collected at 0.3 ps after excitation. Features corresponding to the PVB Pg GSB centred at 532 nm, as well as ESA features at 440, 496, and 663 nm are clearly defined. These features remain in SADS2 which displays an additional positive feature, which we ascribe to the first reaction intermediate at 555 nm. There are also less intense components at 525, 604, and 648 nm, which may be 'real' features, but are more likely to be artefacts from scattered pump light, residual signal from the 'inactive' protein, and the very low signal levels. SADS3 decays in parallel to the SADS1 to SADS2 conversion and has features similar, although not identical, to SADS1 and SADS2 at 407, 438, 483, 554, 581 and 685 nm. The most significant difference is the large negative feature at 641 nm, corresponding to inactive or modified protein as observed previously [7].

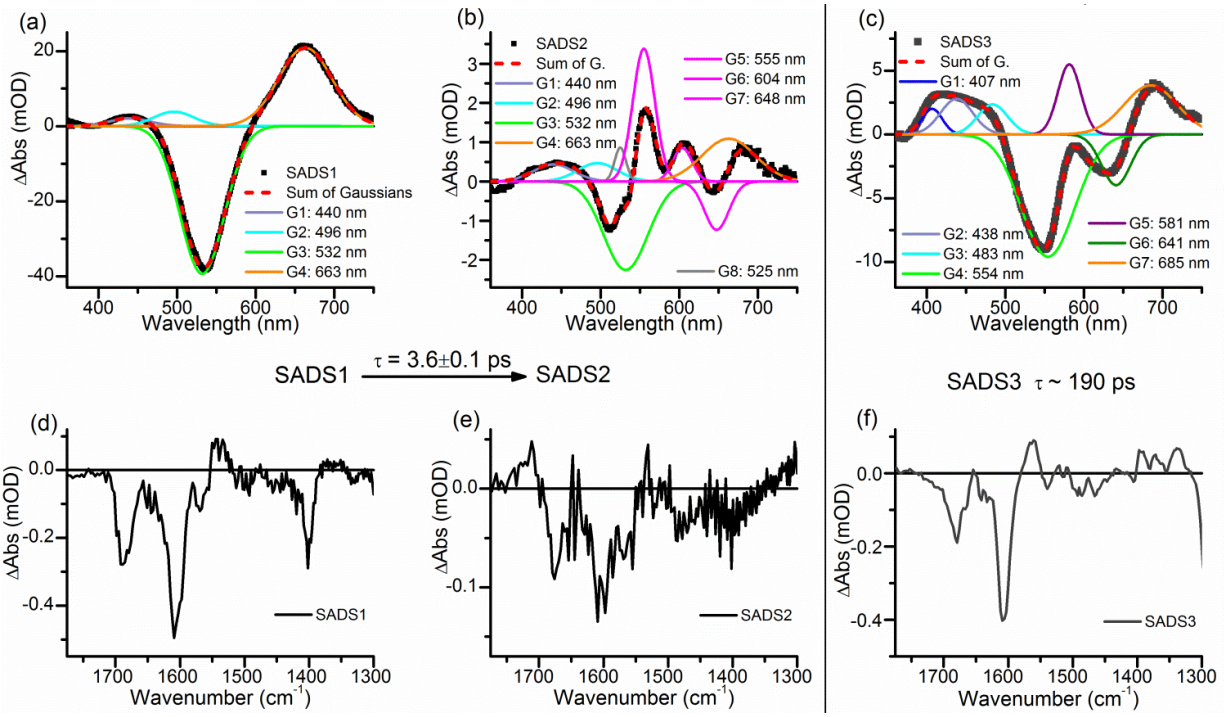

Figure 9. Global analysis of the ultrafast visible (a-c) and IR (d-f) transient absorption data showing resulting SADS (black). The visible TA SADS are fitted with a sum of Gaussian functions (dashed red). The features of SADS1 (a) and SADS2(b) are assigned as: GSB of the PVB Pg state at 532 nm (green), ESA features at 440, 496, and 663 nm (lilac, cyan and orange), intermediate states at 550, 604, and 648nm (pink), and pump scatter at 525 nm (grey). SADS3, representing inactive or modified protein has additional peaks at 641 nm (dark green) and 581 nm (purple).

The SADS resulting from analysis of the IR TA data support the species assignments of the visible TA analysis. SADS1 displays the 3 major bleach peaks observed in the raw data. In addition to the features observed in SADS1 there is a small, but significant positive feature at ~1711 cm^{-1} in SADS2. This correlates well with ultrafast IR TA measurements on the forward photoconversion of PVB from the Pb state where, shortly after photoexcitation a downshift was observed in the same C=O stretching feature, from ~1700 to ~1686 cm^{-1}, which is assigned to the isomerisation reaction [7]. In parallel to the SADS1 to SADS2 conversion, SADS3 decays with a lifetime of 194 ps. This spectrum confirms the assignment of this independently decaying component as a modified version of the chromophore. Whilst SADS1 and SADS2 do appear similar SADS3 completely lacks the N-H in plane bending mode bleach at ~1402 cm^{-1}, and the C=O stretching feature at ~1686 cm^{-1} in SADS1 appears to have downshifted to ~1680 cm^{-1}.

Conclusions

We have used a combination of time-resolved UV-vis and IR measurements to study the *Z* to *E* and *E* to *Z* photoisomerisation processes in the full-length Tlr0924 CBCR. During the photoisomerisation of the 15*Z* species there is a very fast relaxation to the energy minima of the S1 surface in approximately 2 ps. The system then relaxes to either the 15*Z* or 15*E* isomers on a timescale of ~10 ps. After photoexcitation of the of the 15*E* species the majority of the excited state population relaxes back to the ground state with a lifetime of

0.6 ps. A small proportion of the excited population isomerises with a lifetime of 3.6 ps to the *15Z*-PVB, with an absorption maxima at 555 nm.

Acknowledgements

This work was supported by the Biotechnology and Biological Sciences Research Council (BBSRC). S.H. is a BBSRC David Phillips Fellow. N.S.S. is a Wolfson Merit Award holder and holds an Engineering and Physical Sciences Research Council (EPSRC) Established Career Fellowship. The TRIR measurements were carried out through program access support of the Science and Technology Facilities Council.

References

1. M. Ikeuchi and T. Ishizuka, *Photochem. Photobiol. Sci.*, 2008, **7**, 1159-1167.
2. R. Narikawa, T. Ishizuka, N. Muraki, T. Shiba, G. Kurisu and M. Ikeuchi, *Proc. Natl. Acad. Sci. U. S. A.*, 2013, **110**, 918-923..
3. N. C. Rockwell, S. S. Martin, A. G. Gulevich, and J. C. Lagarias, *Biochemistry* 2012, **51**, 1449-1463.
4. Y. Hirose, N. C. Rockwell, K. Nishiyama, R. Narikawa, Y. Ukaji, K. Inomata, J. C. Lagarias and M. Ikeuchi, *Proc. Natl. Acad. Sci. U. S. A.*, 2013, **110**, 4974-4979.
5. T. Ishizuka, A. Kamiya, H. Suzuki, R. Narikawa, T. Noguchi, T. Kohchi, K. Inomata and M. Ikeuchi, *Biochemistry*, 2011, **50**, 953-961.
6. E. S. Burgie, J. M. Walker, G. N. Phillips, Jr. and R. D. Vierstra, *Structure*, 2013, **21**, 88-97.
7. N. C. Rockwell, S. L. Njuguna, L. Roberts, E. Castillo, V. L. Parson, S. Dwojak, J. C. Lagarias and S. C. Spiller, *Biochemistry*, 2008, **47**, 7304-7316.
8. C. C.Cornilescu, G. Cornilescu, E. S. Burgie, J. L. Markley, A. T. Ulijasz, and R. D. Vierstra, *J. Biol. Chem.* 2014, **289**, 3055-3065
9. S. Yoshihara, T. Shimada, D. Matsuoka, K. Zikihara, T. Kohchi and S. Tokutomi, *Biochemistry*, 2006, **45**, 3775-3784.
10. T. Ishizuka, R. Narikawa, T. Kohchi, M. Katayama, and M. Ikeuchi, *Plant Cell Physiol.* 2007, **48**, 1385-1390.
11. L. H. Freer, P. W. Kim, S. C. Corley, N. C. Rockwell, L. Zhao, A. J. Thibert, J. C. Lagarias and D. S. Larsen, *J. Phys. Chem. B*, 2012, **116**, 10571-10581.
12. G. A. Gambetta and J. C. Lagarias, *Proc. Natl. Acad. Sci. U. S. A.* 2001, **98**, 10566-10571.
13. D. J. Heyes, B. Khara, M. Sakuma, S. J. O. Hardman, R. O'Cualain, S. E. J. Rigby and N. S. Scrutton, *PLoS One*, 2012, **7**, 13.
14. A. R. Jones, H. J. Russell, G. M. Greetham, M. Towrie, S. Hay and N. S. Scrutton, *J. Phys. Chem. A*, 2012, **116**, 5586-5594.
15. J. J. Snellenburg, S. P. Laptenok, R. Seger, K. M. Mullen and I. H. M. van Stokkum, *Journal of Statistical Software*, 2012, **49**, 1-22.
16. M. Lorenc, M. Ziolek, R. Naskrecki, J. Karolczak, J. Kubicki and A. Maciejewski, *Appl. Phys. B: Lasers Opt.*, 2002, **74**, 19-27.
17. M. A. Mroginski, F. Mark, W. Thiel and P. Hildebrandt, *Biophys. J.*, 2007, **93**, 1885-1894.
18. J. Dasgupta, R. R. Frontiera, K. C. Taylor, J. C. Lagarias and R. A. Mathies, *Proc. Natl. Acad. Sci. U. S. A.*, 2009, **106**, 1784-1789.
19. K. C. Toh, E. A. Stojkovic, A. B. Rupenyan, I. H. M. van Stokkum, M. Salumbides, M.-L. Groot, K. Moffat and J. T. M. Kennis, *J. Phys. Chem. A*, 2011, **115**, 3778-3786.
20. P. Piwowarski, E. Ritter, K.-P. Hofmann, P. Hildebrandt, D. von Stetten, P. Scheerer, N. Michael, T. Lamparter and F. Bartl, *ChemPhysChem* 2010, **11**, 1207-1214.
21. F. Andel, J. C. Lagarias and R. A. Mathies, *Biochemistry* 1996, **35**, 15997-16008.
22. J. J. van Thor, K. L. Ronayne and M. Towrie, *J. Am. Chem. Soc.*, 2007, **129**, 126-132.
23. H. Foerstendorf, E. Mummert, E. Schäfer, H. Scheer and F. Siebert, *Biochemistry* 1996, **35**, 10793-10799.
24. H. Foerstendorf, C. Benda, W. Gärtner, M. Storf, H. Scheer and F. Siebert, *Biochemistry*, 2001, **40**, 14952-14959.
25. P. W. Kim, L. H. Freer, N. C. Rockwell, S. S. Martin, J. C. Lagarias and D. S. Larsen, *Biochemistry*, 2012, **51**, 619-630.
26. P. W. Kim, N. C. Rockwell, L. H. Freer, C.-W. Chang, S. S. Martin, J. C. Lagarias and D. S. Larsen, *J. Phys. Chem. Letts* 2013, **4**, 2605-2609.
27. M. Bischoff, G. Hermann, S. Rentsch and D. Strehlow, *Biochemistry*, 2001, **40**, 181-186.
28. N. C., Rockwell and J. C. Lagarias, *ChemPhysChem* 2010, **11**, 1172-1180.
29. I. Chizhov, B. Zorn, D. J. Manstein and W. Gärtner, *Biophys. J.* 2013, **105**, 2210-2220.
30. J. Salewski, F. V. Escobar, S. Kaminski, D. von Stetten, A. Keidel, Y. Rippers, N. Michael, P. Scheerer, P. Piwowarski, F. Bartl, N. Frankenberg-Dinkel, S. Ringsdorf, W. Gaertner, T. Lamparter, M. A. Mroginski and P. Hildebrandt, *J. Biol. Chem.*, 2013, **288**, 16800-16814.